Tribological And Corrosion Resistance of Food Grinding Discs: Effects of Ferrochromium

J. A. Adebisi[1], I. I. Ahmed[1], J. K. Odusote[1], A. A. Oyebola[1], A. A. Raji[1], O. L. Jolayemi[1], P. Samuel[1], D. G. Olorunpomi[1], A. A. Owoade[1*], O. F. Oyekoya[1], P. A. Ilesanmi[1], A. O. Odewole[1], M. Dasuki[1], S. Abdulkareem[2]

[1]Department of Materials and Metallurgical Engineering, University of Ilorin, Ilorin, Nigeria.
[2]Department of Mechanical Engineering, University of Ilorin, Ilorin, Nigeria.

ABSTRACT: The pervasive use of cast-iron grinding discs in domestic food preparation poses a dual challenge of material degradation and food safety risks due to tribo-corrosive wear. This study presents the effects of ferrochromium tribological and corrosion resistance of food grinding discs. The study examined a sustainable solution by engineering high-performance, chromium-alloyed grinding discs from upcycled Toyota Engine Block (TEB) scrap. The influences of varying Fe-Cr additions on the microstructure, mechanical properties, and corrosion resistance of the resultant cast irons, which were normalized at 650°C and 850°C were systematically investigated. A comprehensive suite of characterization techniques, including hardness, tensile, wear, and impact testing, supplemented by SEM-EDS, XRF, and XRD analysis, reveals that chromium addition facilitates the formation of protective carbides and a stable passive layer. The results demonstrated a significant enhancement in performance: hardness and yield strength increase substantially, leading to a marked reduction in wear rate and a profound inhibition of corrosion susceptibility, as quantified by gasometric and potentiodynamic polarization methods. This work establishes a robust pathway for transforming industrial waste into superior, food-safe components, with direct implications for enhancing product longevity, reducing environmental footprint, and mitigating contamination risks in consumer appliances.

KEYWORDS: grinding; disc; ferrochromium, cast iron; wear; corrosion.

[Received Jan. 8, 2025; Revised Nov. 30, 2025; Accepted Dec 5th, 2025] Print ISSN: 0189-9546 | Online ISSN: 2437-2110

I. INTRODUCTION

Size reduction is a common food processing method, especially for grains and vegetables, often conducted before consumption. Traditionally, tools like stones (Ehiri *et al.*, 2010; Richard *et al.*, 2010; Anthony *et al.*, 2013) and pestle and mortar (Nnaji and Emmanuel, 2016a) were used. While effective to some extent, these methods are inefficient, time-consuming, and energy-intensive. The growing population necessitated faster and more efficient techniques, leading to the development of a longstanding technology that employs two grooved cast-iron discs rubbing together. This mechanism, still widely used for food grinding today, has inherent drawbacks, including tribological wear and galvanic corrosion when exposed to water. These issues can cause the grinding discs to deteriorate, potentially contaminating processed food with metal particles, and posing significant health risks. According to the World Health Organization (WHO), approximately 10% of the global population suffers foodborne illnesses annually, resulting in around 420,000 deaths (World Health Organization, 2015). In many African and Asian households, reliance on grinding discs to process staple grains like millet and sorghum, and the consumption of food contaminated with metal fragments, represent serious health hazards (Odusote *et al.*, 2017; Anyanwu *et al.,* 2018; Laoye *et al.*, 2025). Addressing this issue will reduce contaminants in processed food significantly.

Predominantly, grinding discs are made from cast iron containing iron, carbon, silicon, and other alloying elements which may include heavy metals, known to be carcinogenic (Ehiri *et al.*, 2010; Anthony *et al.*, 2013). Recent studies by Odusote *et al.* (2016 and 2017) on the assessment of quantity and quality of the contaminants in wet and dry ground food confirmed that not less than 1.4 g of iron filings (around 12 nm grain size) were discovered in 1 kg of ground food using local grinding machine.

Concerted efforts have been made to address the challenges associated with metallic contamination in ground food, including the incorporation of misalignment detecting sensors and signalling apparatus (Normanyo *et al.*, 2009; Yahaya *et al.*, 2012; Aldrich, 2013; Anthony *et al.*, 2013; Isalkar, 2014; Nnaji and Emmanuel, 2016b; Nnaji *et al.*, 2020). Addressing this issue also requires urgent measures, such as modifying the alloy composition of grinding discs. This approach has already been explored in the sugar industry, where modifications to

*Corresponding author: abdurrauf334@gmail.com

doi: http://dx.doi.org/10.63746/njtd.v22i4.3272

grey cast iron have successfully enhanced grinding media performance and reduced contamination. (EL-Sawy *et al.*, 2017). This research investigated the effects of ferrochromium alloy additions on the wear degradation and corrosion susceptibility of grinding discs produced from recycled cast iron.

II. METHODOLOGY

A. Materials

Cast iron from scrapped Toyota Engine Blocks (TEB) (Figure 1a) were obtained from Pata Oloje scrap market in Ilorin, Kwara State, and ferrochromium (Fe-Cr) alloy (Figure 1b) obtained from Akure, Ondo State, are the materials used for this research. The reference material is a grinding disc as presented in Figure 1c. Other materials include premium motor spirit (PMS), rotary furnace at the Department of Materials and Metallurgical Engineering Foundry Workshop, University of Ilorin, and green sand mould.

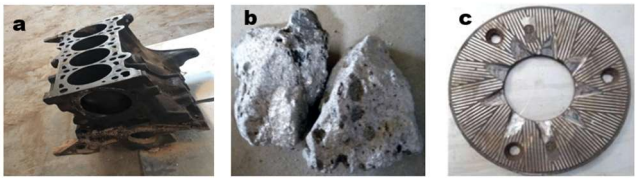

Figure 1 (a)Toyota engine block (TEB), (b) ferrochromium alloy, and (c) grinding disc

B. Methods

Recycled cast iron was sourced from fragmented (manually using a sledgehammer) and solvent-degreased (PMS) TEB scraps. All melts were conducted in a preheated rotary furnace, with sand moulding employed for all castings. A control alloy was first produced from a 25 kg charge of TEB scrap. Subsequently, Fe-Cr was introduced to create two alloyed variants by charging 24.75 kg of TEB scrap with 250 g of Fe-Cr, and 24.625 kg of TEB scrap with 375 g of Fe-Cr, respectively (Table 1).

Table 1 Charge composition

Fe-Cr (%)	Engine Block (%)	Cumulative mass of Fe-Cr (kg)	Residual mass of Engine Block (kg)
0.00	100.00	0.000	25.000
1.00	99.00	0.250	24.750
1.50	98.50	0.375	24.625

1. Heat Treatment

Cast samples with and without Fe-Cr addition were subjected to heat treatment at 650°C and 850°C, soaked for 4 hours, removed the samples, and air-cooled at room temperature. The heat treatments were carried out to reduce excessive hardness gained from the alloy addition for improved toughness against wear degradation and fatigue (Straffelini *et al.*, 2016).

2. Chemical Composition

Metallographic sample preparations of cast samples were carried out by sequential grinding and polishing, with abrasive papers of various grit sizes and polishing clothes containing diamond pastes, respectively. The polished samples were then examined using Scanning Electron Microscope (SEM) with model number Joel JSF-7600F, as a precursor to the determination of their chemical compositions by Energy Dispersive Spectroscopy (EDS). A secondary electron image was acquired at an accelerating voltage of 15 keV and a working distance of 10.4 mm. Qualitative assessment of chemical composition was carried out with the aid of EDS Bruker Quantax software. EDS relied on an interaction of X-ray excitation with the sample for the analyses. High-energy electron beam was sent and focused on the sample's surface; this produced X-ray spectra from the SEM scan area, while diffracted ray was sent into the detector; the output pulses proportional in height to the X-ray photon energy are exhibited as a count (number of X-rays received and processed by the detector) on the vertical axis, and the energy level of those counts are on the horizontal axis. Each element produces characteristic X-rays at different energy levels.

Furthermore, the quantitative assessment of the elemental chemical composition was also carried out using XRF Mini Pal 4 version PW 4030 operated at 30 keV (Jamok *et al.*, 2014). Cast samples subjected to metallographic sample preparation were examined using XRF spectrometer installed with Mini Panalytical software. The software helps in qualitative and quantitative chemical composition analyses.

3. Phase Identification

XRD was carried out using Panalytical Empyrean X-ray Diffractometer to detect phases that evolved after alloying with Fe-Cr. Copper (Kα-XRD-740) anode radiation tube was used. A divergence and scatter slit of 1.0° each and a receiving slit of 0.3 mm were used. The power rating of the X-ray generator used was 40 mA and 45 kV. Samples were examined at ambient temperature. X-ray intensities were measured at diffraction angles (2θ) between 15° and 75° at a scanning speed of 10°/min, 0.1° pitch, and preset time of 0.6 s (Cullity and Stock, 2001; Ahmed *et al.*, 2018).

4. Hardness Test

Brinell hardness test was carried out following ASTM E10 (ASTM, 2004b) testing procedures. Metallographic sample preparations were carried out on test specimens to obtain a smooth surface prior to hardness test. Diamond ball of 10 mm diameter was used to make indention with applied load of 3000 kgf on the test specimens for 15s. The diameter of indentation produced was measured for calculation of Brinell Hardness Number (BHN) in kgf/mm^2 according to Equation 1.

$$Brinell\ Hardnss\ Number\ (BHN) = \frac{2P}{\pi D(D-\sqrt{D^2-d^2})} \quad (1)$$

Where P is the load (kgf), D is the steel ball diameter (mm), d is the indentation diameter (mm).

5. Tensile Test

The tensile test was conducted according to the ASTM E8 Standard procedures (ASTM, 2004d). The samples were machined to a "dog bone" shape as shown in Figure 2.

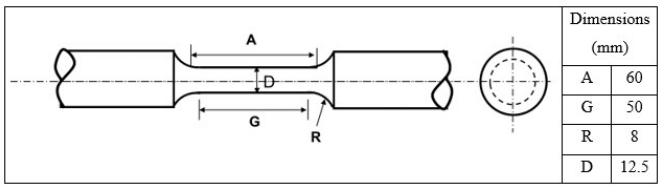

Dimensions (mm)	
A	60
G	50
R	8
D	12.5

Figure 2 Tensile testing specimen ("dog bone") with dimensions

The mechanical tensile testing was carried out on 1000 kN Testometric (AT Model 1000 kN) universal Testing Machine equipped with WinTest Analysis software for test and analysis of results. The cross-head speed used was 8.34×10^{-2} mm/s. The sample was then held in test position with wedge grips and uniaxially loaded to 1% strain to determine the yield strength of the materials. The applied force and elongation were recorded from which tensile stress and strain were calculated automatically by the machine. Though, the strength of materials obtained did not represent the absolute values since strain gauge could not be used for strain measurement. However, the data obtained were sufficient for characterisation and comparative analysis with respect to Fe-Cr alloy addition.

6. Wear Degradation Test

A wear test was carried out using a pin-on-disk tribometer with a rotary stage according to ASTM G99 standard procedure (ASTM, 2004c). The specimens were pinned on the wear testing machine one after the other under the same load, speed, and time. Loads of 7.5 N and 10 N were applied at a rotating speed of 200 rpm in a dry condition for a duration of 60 seconds at ambient temperature. The specimens were weighed before and after the test using a digital weighing balance to determine the specimens' mass loss. The specific wear rate (W_S), the volume of material removed per unit load per unit sliding distance at specific conditions, was estimated using Equation 2.

$$Specific\ wear\ rate\ (W_S, mm^3/N\cdot m) = \frac{V}{F\times D} \qquad (2)$$

Where V is the wear volume loss (mm^3), F is the applied normal load (N), D is the total sliding distance (mm).

7. Impact Energy

Fracture toughness tests were subsequently carried out on the two sets of heat-treated samples using Izod impact test machine. The samples were machined to standard Izod impact geometry with dimensions 90 × 10 × 10 mm (L × W × H) and a V-notch of 2 mm depth at angle 45° to the centre of the sample according to the ASTM E 23 standard (ASTM, 2003). The test sample was supported by a vice (cantilever beam) with the notch facing the direction of the striker. The striker was well fitted in the hammer and the latching position set to 90°C, the hammer was then released to strike the sample. The impact energy of the sample was measured and correlated with amount of Fe-Cr addition and heat treatment temperature.

8. Corrosion Test

Corrosion behaviour of the samples was examined using gasometry and potentiodynamic polarization scan methods. Gasometry measures hydrogen gas evolution from corroded samples during immersed in acid over a given time. Gasometric is a quick test to assess the effect of Fe-Cr addition on corrosion characteristics of the cast samples. Coupons of control and alloyed samples were immersed in 100 ml of 4 M HCl solution for 4 hours, while the quantity of water displaced by the hydrogen gas evolved was recorded.

In addition, corrosion susceptibilities of the cast samples were also assessed using electrochemical method according to ASTM G61 (ASTM, 2004a). Potentiodynamic polarization scan was carried out in a 200 ml standard three-electrode electrochemical cell using VersaSTAT 4 Potentiostat with installed software. Metallographic sample preparation was done before the scanning. With 1 cm^2 sample sizes as working electrodes, platinum wire was used as a counter electrode, and Ag/AgCl in KCl (saturated calomel) electrode served as a reference electrode. Open circuit potential measurement was recorded for 30 min with a scan rate of 0.2 mV/s from -1.5 to -0.5 V in 0.5 M H_2SO_4 at ambient temperature (Ahmed *et al.*, 2015c).

III. RESULTS AND DISCUSSION

A. Composition Analysis with EDS and XRF

The results of compositional assessment of cast samples containing 1.5 wt.% Fe-Cr addition obtained from SEM/EDS is shown in Figure 3 and is typical of other test samples. The most prominent spectrum in Figure 3 was iron, Fe which represents the host atom in the alloy composition. A number of other spectral observed in the EDS results revealed the presence of the alloying elements including silicon and chromium which were also prominent among the spectra observed in the cast samples. Others include Al, S, K, Ti, Ag, Mn, Na, Cl, C, Y, and Nb.

The elemental composition of the cast samples is shown in Table 2. As expected, iron is the dominant element containing 88.46, 88.94, and 88.14 wt.% for the control sample, 1.0 wt.%, and 1.5 wt.% Fe-Cr addition, respectively. Their respective chromium contents were 0.08, 0.28, and 0.95 wt.%, respectively. The results showed that chromium content in the control sample increased proportionally with increase in Fe-Cr addition to other alloys.

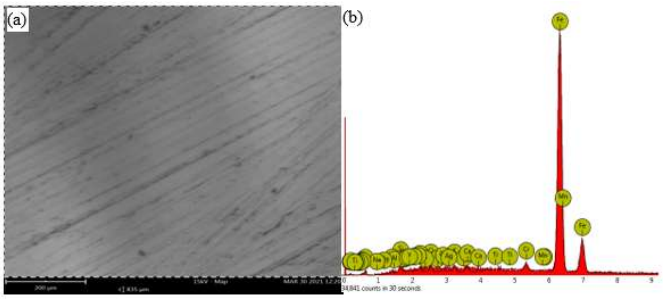

Figure 3 (a) SEM image and (b) Energy dispersive spectrometer of cast samples with 1.5 wt.% Fe-Cr addition

Table 2 Chemical composition of samples produced from different ferrochromium additions

Charge Composition		Elemental Composition (wt.%) Fe	Cr	Si	Al	S	K	Mn	Cu	Pb
Control	100% TEB	88.46	0.08	2.48	3.12	0.18	0.14	0.4	0.02	0.02
1.0 wt.% Fe-Cr	99.0% TEB	88.94	0.28	1.20	1.24	0.11	0.08	0.3	0.03	0.04
1.5 wt.% Fe-Cr	98.5% TEB	88.14	0.95	2.42	2.75	0.27	0.13	0.3	0.01	0.04

B. X-Ray Diffraction

The XRD results are shown in Figure 4. It presented diffraction spectra of control, 1.0 wt.% and 1.5 wt.% Fe-Cr samples. The control and alloyed samples showed one prominent spectrum which was identified to be α-phase (Fe) with a slight shift in peak position of sample with Fe-Cr addition compared to control sample.

However, the presence of α (Fe) and γ (Fe-Cr) phases were quite obvious in samples with 1.0 wt.% Fe-Cr and 1.5 wt.% Fe-Cr additions and these phases suggests the presence of iron and carbides of iron and chromium respectively at 44.5°. The α and γ peaks were quite dominant at this peak position which is consistent with the report of El-Shawy *et al.* (2017). The formation of carbides phases with Fe-Cr addition is not unexpected due to high affinity of carbon for Fe and Cr (Atanda *et al.*, 2010; Agunsoye *et al.*, 2013). Other peaks identified particularly in samples with 1.5 wt.% Fe-Cr addition are β ($MgFe_2O_3$) and δ ($Fe_{2.5}O_4Ti_{0.52}$) phases. Again, the observed peak shift in samples with Fe-Cr addition compared with the control sample could be attributed to the lattice distortion caused by the presence of chromium alloy in the host atom of iron.

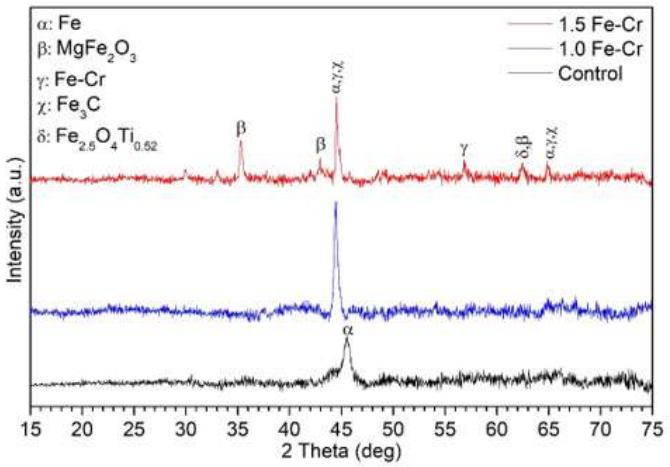

Figure 4 X-ray diffractometry of cast samples with varying Fe-Cr addition

C. *Hardness*

The results of hardness values are shown in Figure 5, the Brinell hardness numbers observed in control, 1.0, and 1.5wt.% Fe-Cr samples are 543, 579, and 600 kgf/mm^2, respectively. The result showed that hardness increases with an increase in Fe-Cr addition. The observed increase in hardness number with Fe-Cr addition may be related to the formation of hard and brittle carbide phases (e.g., Cr_7C_3) because of the high affinity of chromium for carbon (Atanda *et al.*, 2010). Chromium's primary role in cast iron is to form hard carbides that resist abrasion and deformation (Fu *et al*., 2008). This observation is consistent with the XRD results which revealed the presence of γ (Fe-Cr) phase spectrum identified as carbides of chromium and iron.

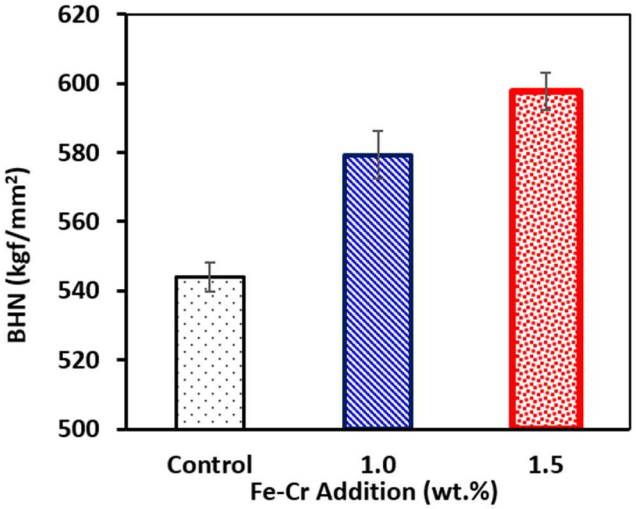

Figure 5 Effect of ferrochromium addition on hardness values

D. *Tensile Test*

The results of tensile tests in Figure 6 showed the stress-strain plots for control, 1.0 wt.% Fe-Cr and 1.5 wt.% Fe-Cr samples. The control sample without Fe-Cr addition recorded a yield strength of 10 MPa and 1.0wt.% Fe-Cr sample recorded a yield strength of 15 MPa, while, 1.5wt.% Fe-Cr sample has a yield strength of 28 MPa. The yield strengths are in concord with increase in chromium addition. Hence, the yield strength of materials increased consistently with increase in Fe-Cr addition. El-Shawy *et al.* (2017) presented similar observation that increase in chromium content increases the ultimate tensile strength of cast iron. Complementary increment in hardness and tensile strength of a materials will increase the toughness in service. This is a desirable improvement in service property of grinding discs.

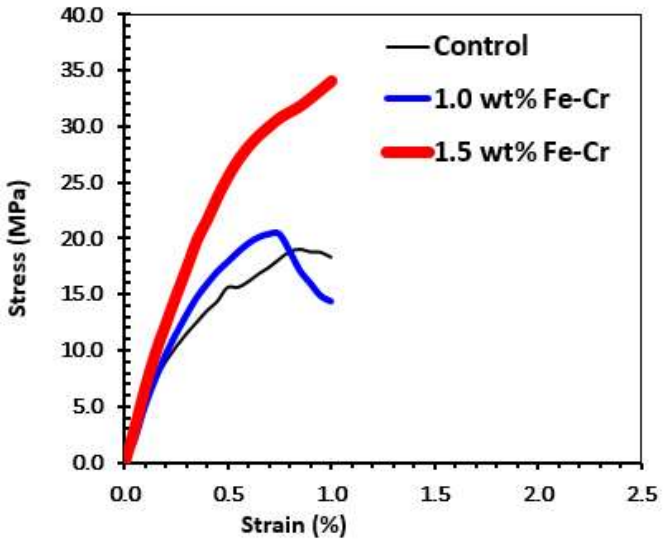

Figure 6 Effect of ferrochromium addition on the strength of cast iron

E. *Wear Test*

The results of wear degradation test are shown in Figure 7 (a) as plot of wear loss against Fe-Cr addition. The trend of wear test results is consistent with the previous mechanical test carried out. It was observed that increase in Fe-Cr addition translated to decrease in wear mass loss for the different loads applied. Again, it was also observed that higher load of 10 N produced greater wear mass loss in all samples than load of 7.5 N. The effect of applied load on the control sample, without Fe-Cr addition was relatively higher compared to samples with Fe-Cr addition, while effects of applied loads become less significant with increasing Fe-Cr addition.

The observed slope at 10 N applied load is 10 times that observed at 7.5 N, as shown in Equations 3 and 4, respectively, where y is the wear loss (g) and x represents Fe-Cr addition. From the linear regression models, the negative slopes indicate that chromium addition reduces wear loss irrespective of the applied load and thus has a strong beneficial effect on the cast iron alloy.

$$y = -0.0237x + 0.0984 \quad (R^2 = 0.614) \qquad (3)$$

$$y = -0.0024x + 0.0444 \quad (R^2 = 0.794) \qquad (4)$$

Figure 7 (b) presents the specific wear rate against the Fe-Cr addition (in wt.%) for two different normal loads: 10 N and 7.5 N. The specific wear rate is a normalized parameter (mm³/N·m) that allows for a direct comparison of material wear resistance under different loading conditions. For both applied loads, the specific wear rate decreases as the chromium content increases. This is the most prominent trend in Figure 7(a) and visually confirms the negative slopes from your linear models (-0.0237 and -0.0024). Under the higher 10 N load, chromium addition yields a marked and substantial improvement in wear resistance. The specific wear rate undergoes a pronounced decrease from approximately 9.8 × 10^{-6} mm³/N·m at the baseline (0% Cr) to about 7.2 × 10^{-6} mm³/N·m at 1.6 wt.% Cr. This represents a relative reduction in wear rate of approximately 27%, underscoring the critical role of chromium carbide formation in resisting the more severe wear mechanisms activated under high contact stress. In contrast, the specific wear rate declines only slightly, from ~7.5 × 10^{-6} mm³/N·m to ~7.0 × 10^{-6} mm³/N·m, a relative improvement of just 6.7% for lower load of 7.5 N.

These results suggest that the addition of Fe-Cr may help to reduce the wear degradation of grinding disc, and it is consistent with earlier reports (EL-Sawy *et al.*, 2017). Hence, Fe-Cr alloy additions impart substantial wear resistance to cast iron, a critical property for minimizing abrasive wear and subsequent particulate contamination in food processing applications.

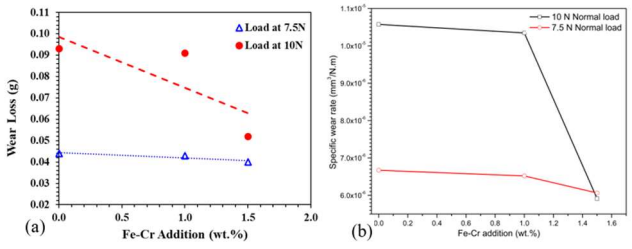

Figure 7 Effect of Ferrochromium addition on (a) wear loss and (b) wear rate at different applied loads

F. *Impact Energy*

It is axiomatic that increase in hardness arising from Fe-Cr addition will undoubtedly translate to loss of impact energy and poor fracture toughness. Therefore, it became necessary to carry out heat treatments that will help to placate the damaging effects of high hardness introduced by Fe-Cr addition. The results of impact tests on heat treated control and alloyed samples are shown in Figure 8 as a plot of impact energy against Fe-Cr addition. Th effect of heat treatment on the cast samples was actually revealed on control sample. The impact energy of 67 J was recorded for control samples at room temperature while 70.2 J and 70.5 J were recorded for heat treated samples at 650 °C and 850 °C, respectively. It was also observed that, samples heat treated at higher temperature of 850 °C recorded relatively higher impact energy compared with samples heat treated at 650°C, for all the samples. The results of heat treatment suggest that, samples alloyed with Fe-Cr which would have ordinarily suffered loss of fracture toughness on account of higher hardness consequent upon chromium alloying effect, now experience significant gain in impact energy as a result of heat treatment. The hard and brittle carbide phases introduced through rapidly cooled sand casting have been successfully modified by heat treatment. Effect of temperature is most pronounced in sample with 1.0% Fe-Cr addition as revealed by highest impact energy of 73 J relative to others with average impact energy of 70.30 ± 0.19 J.

Heat treatment at sub-critical temperature of 650 °C would have facilitated tempering treatment, that would enhance precipitation of tempered carbide over the soaking temperature for 4 hours from supersaturated ferrite phase. On the other hands, the heat treatment above the A1 temperature at austenitizing temperature of 850°C will enhance solid solutioning depending on the magnitude of austenite phase entrapment (gamma loop). Soaking at 850°C for 4 hours is expected to cause enhanced precipitation of carbides of iron and chromium from austenite with greater ease than soaking at 650°C. The precipitation of carbide at soaking temperature is expected to cause proportional decrease in hardness value. Hence it is a balance of probability between high hardness and tempered carbide with reasonable ductility and fracture toughness. The resulting product would be ferrochromium alloyed cast with relatively higher hardness for wear resistance and suitably tempered carbide microstructure for improved fracture toughness. Another secondary benefit of Fe-Cr alloy addition is on the credibility of chromium as a corrosion resistance alloying element.

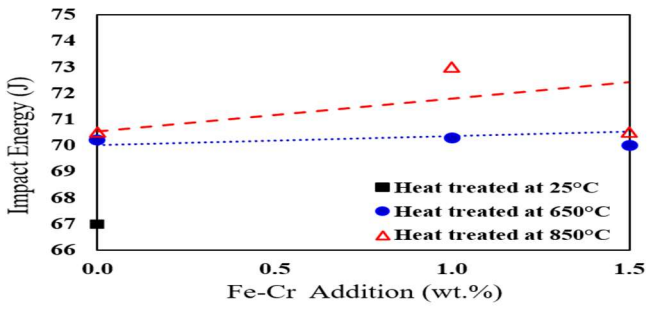

Figure 8 Effects of heat treatment on impact energy of alloyed cast iron

G. *Corrosion*

The grinding disc is made from cast iron and are quite susceptible to corrosion. Thus, it is expected that Fe-Cr addition for wear resistance would translate to better corrosion resistance. Two corrosion measurement techniques were used to assess the gains in corrosion resistance of the samples following Fe-Cr addition.

1. Gasometry

The results of gasometric tests are shown in Figure 9 as a plot of volume of hydrogen gas produced against time. In the first 30 minutes, there was no any observable hydrogen gas evolution from control and alloyed samples exposed to HCl. Not until after 60 minutes, before volume of hydrogen evolution caused water displacement by 2.2 ml and 0.1 ml in control and 1.0 wt.% Fe-Cr sample respectively, while there was no any observable evolution from 1.5 wt.% Fe-Cr sample yet. The higher evolution of hydrogen gas from control sample than alloyed samples was consistent throughout the tests. The observed differences in the hydrogen gas evolution between the control and alloyed samples could be attributed to Fe-Cr addition. Chromium is well-known for its ability to provide protection in corrosive environments by forming a durable chromium oxide film. This film acts as a barrier, shielding the underlying layers from further exposure to harsh environmental conditions (Ahmed *et al.*, 2015a; 2015b; 2015c; Ahmed *et al.*, 2016; Ahmed *et al.*, 2017). Again, it was also observed that after exposure for 180 minutes, there was no remarkable difference in the amount of hydrogen gas evolution between 1.0 wt.% Fe-Cr and 1.5 wt.% Fe-Cr samples. Similarly, during exposure of samples between 210 minutes and end of test duration at 240 minutes, the amount of hydrogen gas evolution from control sample (10.4 ml) remained the same but was still consistently higher than evolution from the alloyed samples (8.8 ml).

These results suggest that, once the minimum threshold amount of chromium for the formation of protective shield is attained, the material becomes protected until the shield is mechanically or chemically damaged and the self-healing may then be subject to amount of chromium accessible for the defence in the alloy. This may have explained the reason why control sample has to remained exposed for up to 210 minutes before attainment of sufficiently stable oxide film to arrest increasing hydrogen gas evolution. The same scenario appeared to have occurred earlier in 1.0 wt.% Fe-Cr sample between 150 and 180 minutes. Hence, these results have demonstrated the capability of chromium alloying for increasing wear resistance as well as reducing the corrosion susceptibility of the grinding disc. However, the protective shield credited to chromium remains vulnerable to mechanical rupture in the case of discs rubbing one another and aggressive chemical infiltration such as chloride from food substances.

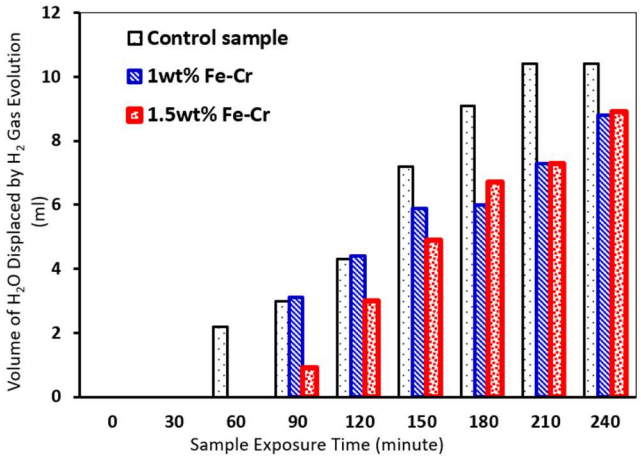

Figure 9 Gasometric results of samples with ferrochromium addition

2. Potentiodynamic Polarization

Figure 10 presents the potentiodynamic polarization scan as a graph of electrode potential versus the saturated calomel electrode against corrosion current density. The plot highlights both the cathodic and anodic regions of the corrosion reaction, indicating the point where the sample is cathodically protected and the onset of corrosion. The corrosion potential (E_{corr}) and corrosion current density (i_{corr}) were determined through Tafel plot extrapolation. The corrosion potentials for the control, 1.0 wt.% Fe-Cr and 1.5 wt.% Fe-Cr samples were measured at -0.91, - 0.74, and - 0.69 mV while their respective corrosion current densities were estimated at 0.000552, 0.000568, and 0.000773 A/cm^2, respectively. The control samples started corroding at -0.91V, the alloyed sample with 1.0 wt.% Fe-Cr started corroding at -0.74V, and the sample with 1.5 wt.% Fe-Cr started corroding at -0.69V, which shows a decreasing order of corrosion susceptibility with an increase in ferrochromium content.

Results from Figure 10 showed that Corrosion Potential (E_{corr}) increases with increasing weight percent of Fe-Cr addition and the higher the corrosion potential, the higher the corrosion resistance of the material. Hence, 1.5 wt.% Fe-Cr sample represents the most noble cast sample and control sample was the least noble cast. This result is consistent with the gasometric test results and therefore confirms that addition of Fe-Cr will not only increase wear resistance of the grinding disc but also reduce its susceptibility to corrosion.

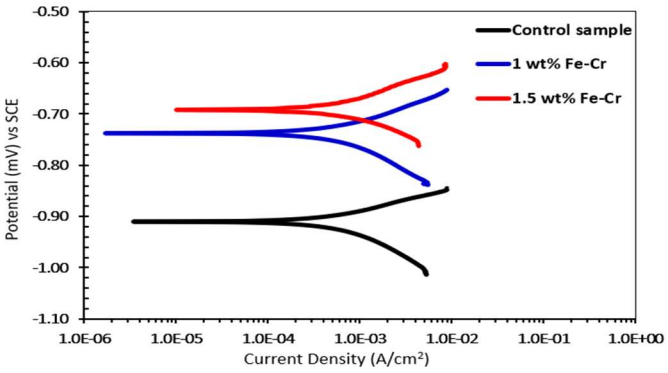

Figure 10: Potentiodynamic polarisation scan of the cast sample with ferrochromium addition

IV. CONCLUSION

The investigation into ferrochromium (Fe-Cr) additions to cast iron for food grinding discs was successfully executed. Chemical analysis confirmed a proportional increase in chromium content. This chromium manifested as a hard $(Fe,Cr)_xC_\gamma$ carbide phase within the alloy's microstructure. The incorporation of these chromium carbides directly resulted in increased hardness and yield strength for the cast alloys. Wear degradation was significantly reduced with higher ferrochromium content, a direct consequence of the increased material hardness. Furthermore, the wear resistance demonstrated a clear dependence on the applied load, performing more effectively under higher loads. The high hardness (and associated brittleness) from Fe-Cr addition was effectively mitigated through heat treatment. This process improved impact toughness, with a higher annealing temperature of 850 °C yielding superior results compared to 650 °C. The addition of ferrochromium provided a dual benefit, significantly enhancing corrosion resistance alongside the previously noted improvement in wear resistance. To evaluate the impact on metallic contamination, we recommend studying how optimizing the composition and manufacturing process of grinding discs.

REFERENCES

Agunsoye, J. O.; T. S. Isaac and A. A. Abiona (2013). On the comparison of microstructure characteristics and mechanical properties of high chromium white iron with the hadfield austenitic manganese steel. Journal of Minerals and Materials Characterization and Engineering. 1(1): 24-28.

Ahmed, I. I.; J. A. Adebisi; S. Abdulkareem and A. H. Sherry (2018). Investigation of surface residual stress profile on martensitic stainless steel weldment with x-ray diffraction. Journal of King Saud University - Engineering Sciences. 30(2): 183-187. https://doi.org/10.1016/j.jksues.2016.01.004.

Ahmed, I. I.; J. A. Adebisi; A. Sulaiman and H. S. Andrew (2017). Analysis of intergranular carbide precipitate in haz of martensitic stainless steel. Journal of Engineering Science and Technology. 12(4): 1037-1047.

Ahmed, I. I.; J. A. Adebisi; T. Yahaya and S. Abdulkareem (2015a). Effects of soaking time and cold work on sensitisation of austenitic stainless steels. Journal of Production Engineering. 18(2): 37-42.

Ahmed, I. I.; J. A. Adebisi; T. Yahaya; I. N. Aremu and A. H. Sherry (2016). Assessment of crack propagation mode in martensitic stainless steel haz with electron back scatter diffraction: Effects of environmental variables. Annals of the Faculty of Engineering Hunedoara - International Journal of Engineering. 14(2): 47-52.

Ahmed, I. I.; A. G. F. Alabi; J. K. Odusote; I. N. Aremu; J. A. Adebisi; T. Yahaya; S. I. Talabi; R. A. Yahya and S. B. Lyon (2015b). Stress corrosion cracking of austenitic stainless steel in chloride environment. Nigerian Journal of Engineering. 21(2): 24-28.

Ahmed, I. I.; T. Yahaya; J. A. Adebisi; I. N. Aremu; A. G. F. Alabi and S. B. Lyon (2015c). Stress corrosion cracking of austenitic stainless steels in potentiostatically controlled chloride environments at ambient temperature. Annals of the Faculty of Engineering Hunedoara - International Journal of Engineering Vol. 13(Issue 4): 151-158.

Aldrich, C. (2013). Consumption of steel grinding media in mills – a review. Minerals Engineering. 49(0): 77-91. http://dx.doi.org/10.1016/j.mineng.2013.04.023.

Anthony, B.; C. Ojekale; G. Chukwu; L. O. Oladipupo and S. O. Titilola (2013). Some Nigerian traditional food milling techniques and cookware increase concentrations of some heavy metals in lycopersicon esculentum and Citrullus lanatus. IOSR Journal of pharmacy, 3(3), 6-13.

Anyanwu, B. O.; A. N. Ezejiofor; Z. N. Igweze and O. E. Orisakwe (2018). Heavy metal mixture exposure and effects in developing nations: an update. Toxics, 6(4), 65.

ASTM (2003). Standard test methods for notched bar impact testing of metallic materials In: Designation: E 23 – 02a. ASTM International, West Conshohocken, USA.

ASTM (2004a). Standard reference test method for making potentiostatic and potentiodynamic anodic polarisation measurements. In: Designation: G5-94. ASTM International, West Conshohocken, USA.

ASTM (2004b). Standard test method for brinell hardness of metallic materials In: Designation: E10-01. ASTM International, West Conshohocken, USA.

ASTM (2004c). Standard test method for wear testing with pin-on-disk apparatus. In: Designation: G99-04. ASTM International, West Conshohocken, USA.

ASTM (2004d). Standard test methods for tension testing of metallic materials [metric]. In: Designation: E 8M-04. 2004. ASTM International, West Conshohocken, USA.

Atanda, P.; A. Okeowo and O. Oluwole (2010). Microstructural study of heat treated chromium alloyed grey cast iron. Journal of Minerals & Materials Characterization & Engineering. 9(3): 263-274.

Cullity, B. D. and S. R. Stock (2001). Elements of X-ray Diffraction. New Jersey: Prentice Hall.

Ehiri, R. C.; U. G. Megwa and O. N. Omaka (2010). Food grinding stones as a source of heavy metal contamination of diets. Journal of Sciences and Multidisciplinary Research. 2.

ELSawy, E.; M. EL-Hebeary and I. El Mahallawi (2017). Effect of manganese, silicon and chromium additions on microstructure and wear characteristics of grey cast iron for sugar industries applications. Wear. 390: 113-124. https://doi.org/10.1016/j.wear.2017.07.007.

Fu, H.; Y. Qu; J. Xing; X. Zhi; Z. Jiang; M. Li and Y. Zhang (2008). Investigations on heat treatment of a high-speed steel roll. Journal of Materials Engineering and Performance, 17(4), 535-542.

Isalkar, U. (2014). Limit for iron filings in tea to stay till may. In: The Times of India.

Jamok, E. J.; Y. Jonathan; M. Abdullahi and K. Matthew (2014). Radiological and x-ray fluorescence spectrometric analyses of selected inorganic fertilizers in zaria kaduna state, nigeria: Source of possible environmental pollution. Int. J. Sci. Res. 3(4): 86-93.

Laoye, B.; P. Olagbemide; T. Ogunnusi and O. Akpor (2025). Heavy metal contamination: Sources, health impacts,

and sustainable mitigation strategies with insights from nigerian case studies. F1000Research, 14, 134.

Nnaji, J.; B. Iweha and I. Ogbuewu (2020). Human health risk assessment of heavy metals in foodstuffs processed with diesel powered metallic disc grinders in umuahia, nigeria. Journal of Chemical Society of Nigeria. 45(3): 458-468.

Nnaji, J. C. and E. P. N. Emmanuel (2016a). Trace metals in food condiments processed with manual metallic grinders. The Phamaceutical and Chemical Journal. 3(1): 172-177.

Nnaji, J. C. and E. P. N. Emmanuel (2016b). Trace metals in food condiments processed with manual metallic grinders. The Pharmaceutical and Chemical Journal. 3(1): 172-177.

Normanyo, E.; E. K. Asiam; K. Amankwa-Poku and I. A. Adetunde (2009). Redesign of a grinding mill for the minimization of iron filings production. European Journal of Scientific Research. 36(3): 418-436.

Odusote, J. K.; G. A. Soliu; I. I. Ahmed; S. Abdulkareem and K. A. Akande (2016). Characterization of metallic contaminants extracted from ground millet. Centrepoint Journal (Science Edition). 22(2;): 57-68.

Odusote, J. K.; G. A. Soliu; I. I. Ahmed; S. Abdulkareem and K. A. Akande (2017). Assessment of metallic contaminants in grinded millet using domestic grinding machine. Nigerian Journal of Technological Development. 14(1): 5. http://dx.doi.org/10.4314/njtd.v14i1.2.

Richard, C. E.; G. M. Ugochukwu and N. O. Omaka (2010). Food grinding stones as a source of heavy metals contamination of diets. Journal of Sciences and Multidisciplinary Research. 2: 113-120.

Straffelini, G.; P. C. Verma; I. Metinoz; R. Ciudin; G. Perricone and S. Gialanella (2016). Wear behavior of a low metallic friction material dry sliding against a cast iron disc: Role of the heat-treatment of the disc. Wear. 348-349: 10-16. https://doi.org/10.1016/j.wear.2015.11.020.

World Helth Organization (2015). Disease outbreak news: Cholra – United Republic of Tanzania. WHO.

Yahaya, D. B.; D. A. Aremu and I. Abdullahi (2012). Investigation of metal contaminants in locally ground foods (beans and tomatoes). Journal of Emerging Trends in Engineering and Applied Sciences. 3(1): 339-343.